Evaluation of free-running ADCs for high resolution PET data acquisition

Hao Peng, *Member, IEEE*, P. D. Olcott , A. M. K. Foudray, C. S. Levin, *Member, IEEE*

***Abstract*– Advances in field-programmable gate arrays (FPGA) allow a larger part of analog circuits to be replaced by digital logic. We are prototyping a high-resolution position-sensitive APD (PSAPD) based PET system, using a fully digital data acquisition system with free-running analog-to-digital converters (ADC) and FPGA logic. Numerical algorithms for digital shaping and digital timing pickup were tested and the results were compared to those obtained by using analog NIM modules for a LSO/PSAPD detector module, in terms of energy resolution, time resolution and positioning ability. A significant improvement in the coincidence time resolution was found using a digital CFD (4.71+/-0.07 ns FWHM) over the analog counterpart (3.15+/- 0.07 ns). A linear time interpolation model provides the best time resolution (1.72+/-0.07 ns).**

I. Introduction

Many existing PET/SPECT scanners are implemented based on analog subsystems with discrete circuits or application specific integrated circuits (ASIC). These solutions yield cost effective results in dedicated systems but offer little flexibility and upgradeability. Currently, advances in field-programmable gate arrays (FPGA) allow a larger part of analog circuits to be replaced by digital logic [1-3]. Replacing analog processing electronics by a fully digital, programmable PET data acquisition scheme would result in the following two advantages: first, the built system can be reconfigured according to different imaging protocols; second, new detector technology such as avalanche photodiode (APD) and cadmium zinc telluride (CZT) can be easily adapted instead of redesigning data acquisition systems.

We are prototyping a high-resolution position-sensitive APD (PSAPD) based PET system [4-5]. The ultimate goal of this project is to implement a fully digital detection system with free-running analog-to-digital converter (ADC) and FPGA logic. Prior to the final implementation, numerical algorithms for digital shaping and digital timing pickup were tested and the results were compared to those obtained by using analog NIM modules.

Manuscript received November 18, 2007. This work was supported in part by grants R01CA120474 from NIH and 12IB-0092 from California Breast Cancer Research Program.

Hao Peng is with the Department of Radiology and Molecular Imaging Program, Stanford University, Stanford, CA. (telephone: 650-736-7093, e-mail: haopeng@stanford.edu).

P. D. Olcott , A. M. K. Foudray, C. S. Levin are with the Department of Radiology and Molecular Imaging Program, Stanford University, Stanford, CA. (telephone: 650-736-7211, e-mail: cslevin@stanford.edu).

II. Material and Methods

A. System architecture and experimental setup

The signals generated by the PSAPD were first passed through an analog preamplifier before they were digitized by the free running ADC. The signal was then compared against a pre-determined threshold and connected to a logic matrix for coincidence selection. If the system generates a coincidence trigger, the system reads out the waveform stored in the buffer and implements digital shaping and digital timing pickup. Unlike traditional PET detection using discrete components or ASICs, all these functions are to be achieved through FPGA programming. In this study, a VHS-ADC-4 (Lyrtech Signal Processing, Montreal, Canada) fully digital system was chosen for the evaluation. The system has an on-board Xilinix Virtex-V FPGA and 8 channels for input. The free-running ADC in the system has 14-bit resolution and can sample up to 108 Mega-samples per second. The stored waveform is then saved for further processing such as pulse shaping and time pickoff (Fig.1).

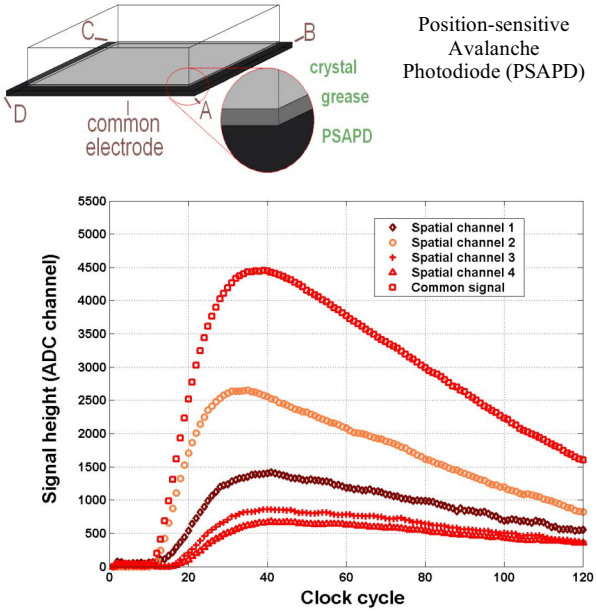

Fig. 1: For a PSAPD, the top common channel is used for extracting energy and time information. Four spatial channels (A-D) are used for position information. Raw waveform capture of five PSAPD channels is shown. The sampling rate is 108 MHz. Such digitized waveforms were used for further processing.

The energy spectrum, coincidence time spectrum and flood source position map were studied. For energy spectrum and position map experiments, an 8x8 mm^2 PSAPD (RMD, Inc.) was coupled to 8 by 8 lutetium oxyorthosilication (LSO) scintillation crystal (with 1x1x1 mm^3 pixels) irradiated by a 10 μCi, 500 μm diameter ^{22}Na point source 5 cm away from the surface of the PSAPD. There are five channels to be detected for each PSAPD. As shown in Fig.1, a top common channel is used for extracting the energy and time information. Four spatial channels (A-D) at the corners of a resistive sheet on the backside of the PSAPD are used for extracting position information of incoming 511 keV photons.

For the timing spectrum, the same ^{22}Na source was used and located equidistant to the PSAPD and a Hamamatsu H3164 standard photomultiplier tube (PMT). The distance between two detectors was approximately 10 cm.

B. *Signal processing algorithm*

The integrated charge from a scintillation event is proportional to the energy of the high-energy photon interaction with the scintillator. Triangular shaping is used for pulse shaping since it is easier to be implemented in FPGA than Gaussian shaping in most analog shaping circuits, as well as being able to minimizing the pulse pile-up effect in PET systems. The triangular filtered output at sample k is the subtraction of two free running averages of length L separated by a gap G, as shown in (1).

$$L \cdot V_{x,k} = -\sum_{i=k-2L-G}^{k-L-G} V_i + \sum_{i=k-L+1}^{k} V_i \qquad (1)$$

A digital constant fraction discriminator (CFD) is used to extract timing information, similar to analog CFD. Such an algorithm can also be easily programmed in to FPGA logic. As shown in (2), for the digital CFD the signal at the k-*th* sample is the running average over L samples of the fraction f times the digitized trace delayed minus the digitized trace. The zero crossing of the digital CFD signal is interpolated back to find the inter-clock arrival time.

$$V_{CFD}(k) = \sum_{i=1}^{L} (f * V_{k-1} - V_{k-i-D}) \qquad (2)$$

Besides digital CFD, two numerical models were used to extract timing information for comparison: a linear model and an exponential model. For both models, the first three points on the pulse rising edge are used to extract pulse arrival time information. A threshold (~1-5% of maximum pulse height) was adjusted and optimized to find the starting position of the pulse prior to the fitting. Four points prior to the starting point were used for baseline restoration.

For the linear model shown in (3), two parameters were fitted (A and B), and then the fitted parameters were substituted to the model to calculate the k value that gives V_{LF} zero value. For the exponential model shown in (4), V_{EXP} is the signal after normalization. Such simplifications enable us to reduce the unknown parameters to k_0 and τ.

$$V_{LF}(k) = Ak + B \qquad (3)$$

$$V_{EXP}(k) = (1 - \exp^{-(k-k_0)/\tau}) \qquad (4)$$

III. RESULTS

A. *Energy resolution*

Using (1), the raw waveform of the common channel from the PSAPD was processed for the triangular shaping. The energy spectrum is shown in Fig. 2, which is the global energy spectrum of the PSPAD and no gain calibration on a crystal basis was done in this study.

Two parameters in (1) were chosen to be G = 5 and L = 10, which provides the optimum shaping linearity and energy resolution. The achieved global energy resolution is 10.3 +/- 0.6% by fitting the experimental data with two Gaussians on a linear background.

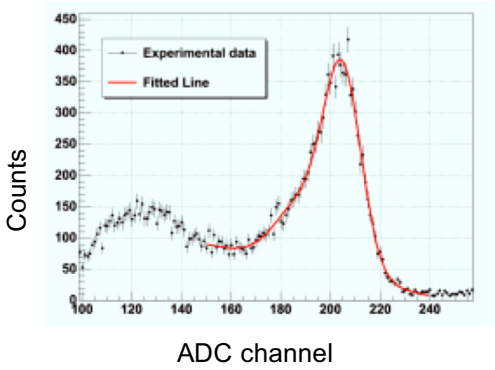

Fig. 2: The global energy spectrum of the LSO array coupled to the PSAPD extracted from the common contact. The X-axis is in ADC channels and Y-axis is in counts.

B. *Coincidence time resolution*

The results of coincidence time resolution using three digital numerical algorithms are presented in this section. For the digital CFD shown in (2), the algorithm and the timing spectrum are shown in Fig. 3. The pulse arrival time was extracted from the zero crossing of the CFD signal. The parameters D, f and L were chosen after the optimization. The achieved time resolution is 4.71 ± 0.07 ns in full-width-half-maximum (FWHM).

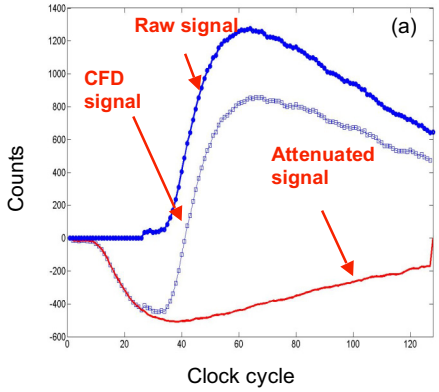

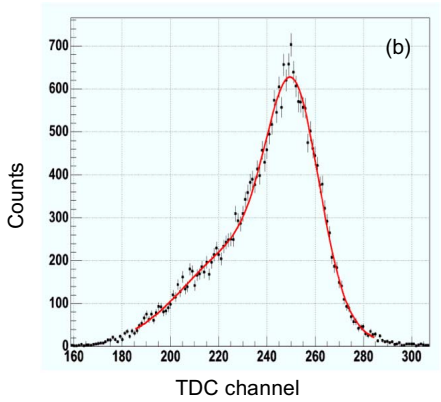

Fig. 3: (a) An example of components needed for digital CFD algorithm. (b) The coincidence time spectrum for digital CFD algorithm. D = 1. f = 0.03. L = 2. Due to different timing responses of PMT and PSAPD, the spectrum was not symmetric and was fitted by the sum of two Gaussian functions. Time-to-digital converter (TDC) channel corresponds to the bin index of the histogram of timing spectrum in the post-processing.

For our digital CFD analysis, both the timing spectrum and time resolution are not significantly affected by the threshold selection (f value), since the delay signal is used in the signal processing. As a result, the effects of baseline wandering and noise are minimized. However, for both linear and exponential model, the timing spectrum shows strong dependence on the threshold selection, which is illustrated in Fig. 4a and 4b. Two side lobes stay on the either side of the main coincidence peak and the temporal shift between adjacent peaks is approximately 1 clock cycle (~ 9.25 ns) of the free-running ADC.

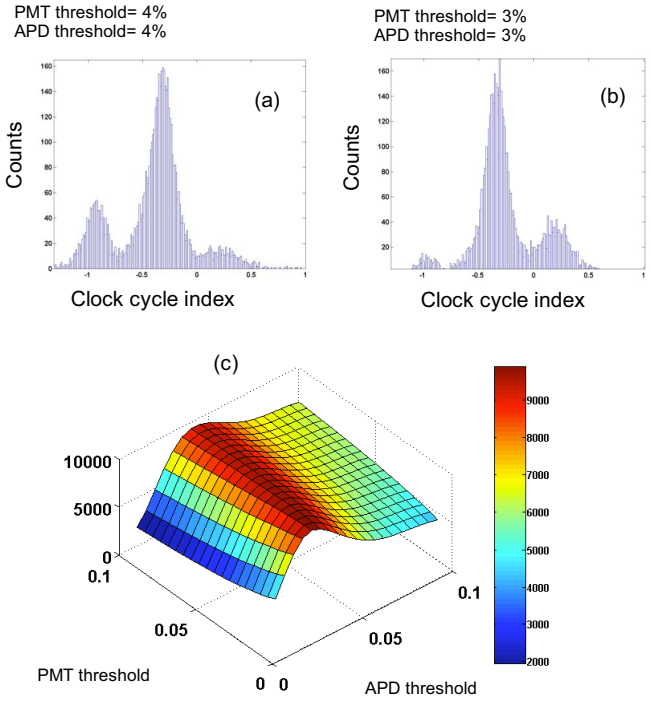

Fig. 4: (a) and (b): The coincidence timing spectrum for different threshold selection. X-axis is in clock cycle index. Y-axis is in counts. The total counts is 10000. (c) Illustration of the optimization routine for threshold determination. The threshold refers to the percent of the peak amplitude of a given raw input signal.

As shown in Fig. 4c, the count under the main coincidence peak was studied as a function of the threshold of PSAPD and PMT. The optimum thresholds were chosen to be 3% for the PSAPD and 2% for the PMT, which corresponds to the condition for achieving the maximum coincidence counts. Using these thresholds, the timing spectra for three algorithms are presents in Fig.5.

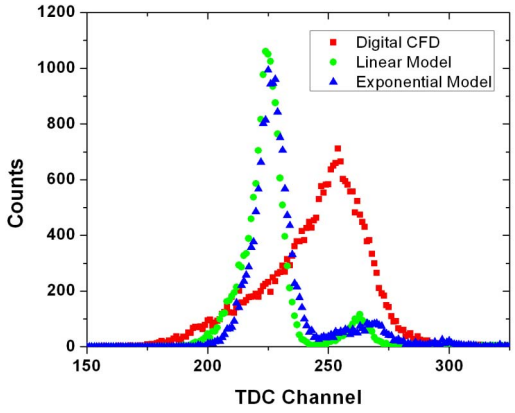

Fig. 5: The timing spectra for all three methods. A narrower peak means the better time resolution. The peak offset between the digital CFD and the other two other models is caused by the delay applied in the CFD algorithm.

C. *Flood source position map*

The four spatial channels were processed for triangular shaping in the same way as that for the common channel. The amplitudes were then used for the positioning study as shown in (5). All 64 crystal pixels were clearly resolved. A cross-section profile for the central column analyzed and the mean peak-to-valley ratio was 6.33± 2.42.

$$X = \frac{A+B-C-D}{A+B+C+D} \qquad Y = \frac{A+C-B-D}{A+B+C+D} \tag{5}$$

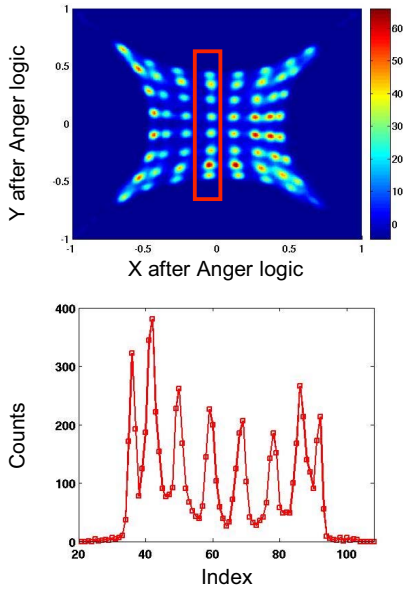

Fig. 6: (Top) Crystal identification (1x1x1mm^3 LSO crystals in an 8 by 8 array. No reflector between crystals was used. Counts: 150, 000. Image size: 128 x 128. (Bottom) The central column in the image (inside the red rectangular) was used to calculate the crystal peak to-valley ratio.

D. Performance comparison

The above results were compared against our previous experiments using NIM systems. For the energy resolution, the global result by digital triangular shaping algorithm is 10.3±0.6% at 511 keV, which is better than our previous result (12.8±0.6%, using a Gaussian plus an exponential background model for fitting) with ORTEC analog NIM modules. The peak-to-valley ratio is 6.33±2.42, which is slightly superior to that obtained by analog NIM modules (5.40±2.9). In terms of the coincidence time resolution, all digital methods show better performance than that of analog NIM CFD shown in Table. 1. The linear model provides the best time resolution in this study.

Table. 1: Timing performance of digital models versus analog CFD

	Time resolution (ns)	
	FWHM (ns)	FWTM (ns)
Digital CFD	4.71 ± 0.07	12.19 ± 0.12
Linear Model	1.72 ± 0.07	4.34 ± 0.12
Exponential Model	2.12 ± 0.04	4.62 ± 0.07
Analog CFD	3.15 ± 0.07	5.73 ± 0.12

IV. SUMMARY

Compared to analog processing circuits, the digital system tested exhibits better energy resolution at 511 kV and crystal peak-to-valley ratio in the flood source position map, for a LSO/PSAPD detector module. A significant improvement in the coincidence time resolution was found using the digital CFD over the analog counterpart, which is in agreement with previous observations for Bismuth-Germanium-Oxide (BGO) coupled to low gain discrete APDs [1]. These improvements may be attributed to the better noise and linearity performance of the digital signal processing.

In addition, the linear model provides the best time resolution. However, the linear method and exponential method are more difficult to implement in FPGA and their performances are also found to be more sensitive to threshold settings and noise, compared to the digital CFD.

ACKNOWLEDGMENT

We would like to thank Lyrtech Digital Systems (Montreal, Canada) for providing the data acquisition system.

REFERENCES

[1] J.D. Leroux, R. Lecomte, et al. “Time determination of BGO-APD detectors by digital signal processing for PET”, IEEE NSS 1723-1727 2003.

[2] M. Streum, et al. “A PET system with the free running ADCs”, Nucl. Instr. Meth. Res. A. 486 18-21 2002.

[3] A. Fallu-Labruyere et al. “Time Resolution Studies using Digital Constant Fraction Discrimination”, presented at the SORMA XI conference, Ann Arbor MI, USA, May 2006.

[4] C.S. Levin, et al. “Investigation of position sensitive avalanche photodiodes for a new high-resolution PET detector design”, Nuclear Science, IEEE Transactions on Nuclear Science, 51, Part 2, 2004.

[5] P.D. Olcott, et al. “A high speed fully digital data acquisition system for Positron Emission Tomography”, IEEE NSS/MIC conference record, 2006.